




Rovibrational quenching of C_2^- anions in collisions with He, Ne, and Ar atoms

Barry P. Mant , Franco A. Gianturco ,* and Roland Wester 

Institut für Ionenphysik und Angewandte Physik, Universität Innsbruck, Technikerstr. 25, 6020, Innsbruck, Austria

Ersin Yurtsever 

Department of Chemistry, Koç University, Rumelifeneri yolu, Sariyer, TR-34450, Istanbul, Turkey

Lola González-Sánchez 

Departamento de Química Física, University of Salamanca, Plaza de los Caídos sn, 37008 Salamanca, Spain



(Received 30 April 2020; accepted 16 November 2020; published 10 December 2020)

The molecular anion C_2^- is currently of interest as a candidate for laser cooling due to its electronic structure and favorable branching ratios to the ground electronic and vibrational states. Helium has been proposed as a buffer gas to cool the molecule's internal motion. We calculate the cross sections and corresponding rates for rovibrational inelastic collisions of C_2^- with He, and also with Ne and Ar, on three-dimensional *ab initio* potential energy surfaces using quantum scattering theory. The rates for vibrational quenching with He and Ne are very small and are similar to those for small neutral molecules in collision with helium. The quenching rates for Ar, however, are far larger than those with the other noble gases, suggesting that this may be a more suitable gas for driving vibrational quenching in traps. The implications of these results for laser cooling of C_2^- are discussed.

DOI: [10.1103/PhysRevA.102.062810](https://doi.org/10.1103/PhysRevA.102.062810)

I. INTRODUCTION

Laser cooling of molecules has become a very active research area [1]. With the direct preparation of ultracold molecular ensembles in magneto-optical traps [2], numerous experiments on molecular quantum control, quantum phases [3], precision spectroscopy [4], or ultracold chemistry [5] become accessible. For atoms, laser cooling of neutral and charged species has developed hand in hand. For molecules, however, no charged molecular species has yet been successfully laser cooled. Ions with bound excited electronic states that lie below the first fragmentation threshold and can be excited with suitable narrow-band lasers are rare. Furthermore, a near-optimal Franck-Condon overlap of the vibrational wave functions is required to make closed optical cycles feasible.

The diatomic carbon molecular anion has been identified as an interesting exception [6], as it possesses several bound excited electronic states below the photodetachment threshold. Furthermore, the electronic states $A^2\Pi_u$ and $B^2\Sigma_u^+$ (Fig. 1) have high Franck-Condon overlap factors with the $X^2\Sigma_g^+$ ground state for the transitions between their lowest vibrational levels $v' = 0 \rightarrow v'' = 0$ [7,8]. Simulations of laser cooling using the $B^2\Sigma_u^+$ [6] and $A^2\Pi_u$ [9] states have both shown that C_2^- can, in principle, be cooled efficiently to millikelvin temperatures using Doppler or Sisyphus cooling in Paul or Penning traps. Photodetachment cooling has also been shown to allow even lower temperatures to be accessed [10]. If laser cooling of C_2^- anions were to be realized, it would open

up the possibility of sympathetically cooling other anions [9] or even antiprotons [10]. This last achievement could allow the efficient production of antihydrogen atoms, currently being investigated for tests of fundamental physics such as CPT invariance [11] and the weak equivalence principle [12].

The diatomic carbon molecular anion C_2^- has been a model system for decades, attracting a great deal of experimental [13–27] and theoretical [8,28–36] work. Its bound electronically excited states [32] are unusual for an anion, which is a consequence of the high electron affinity of neutral C_2 of around 3.3 eV [17,21] in combination with the open shell character of the electronic configuration of carbon dimers. In its ground electronic state $X^2\Sigma_g^+$ the molecule has only evenly numbered rotational states due to the nuclear statistics of the $^{12}C_2^-$ molecule with zero spin nuclei, while in the excited $B^2\Sigma_u^+$ state only odd-numbered rotational states exist.

It has also been suggested that C_2^- could be present in astronomical environments as neutral C_2 is abundant in interstellar space [37], comet tails [38], and is a common component of carbon stars [39,40]. The large EA of C_2 and strong electronic absorption bands of C_2^- [16] suggest that the anion could also be detected in space [41], but as yet no conclusive evidence of its presence has been found [42–44]. As the most abundant isotopologue $^{12}C_2^-$ is a homonuclear diatomic molecule, it does not exhibit a pure rovibrational spectrum, making its detection in emission difficult. Transitions to and from low-lying excited electronic states could, however, allow for the anion's detection or, as will be evaluated and discussed here, as a possible option, for the detection of the $^{12}C^{13}C^-$ isotopologue which would then have a small dipole moment.

*francesco.gianturco@uibk.ac.at

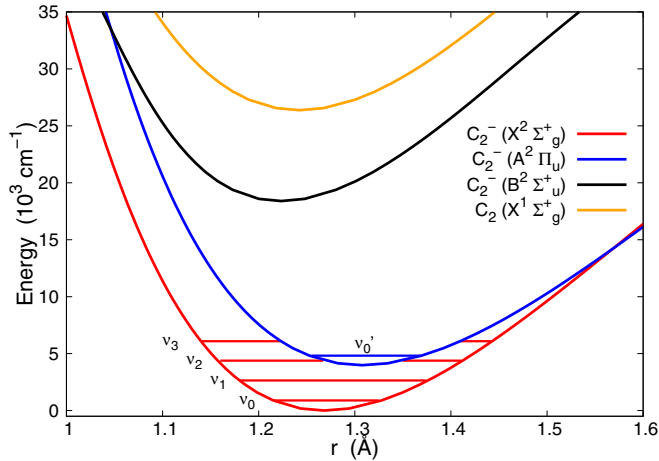


FIG. 1. Potential energy curves for the three lowest-energy electronic states of C_2^- and for the ground state of C_2 . The vibrational levels of interest in this study are also shown. The curves were obtained using the Rydberg-Klein-Rees (RKR) method [51] with the spectroscopic constants from Ervin and Lineberger [21].

Laser cooling of C_2^- would ideally start with ions initially cooled to around 10 K, for example by helium buffer gas cooling in a cryogenic ion trap [45,46]. Processes used to generate C_2^- involve applying an electric discharge to a mixture of C_2H_2 and CO_2 in a carrier gas [25,47] which may form the anion in excited vibrational states. Aside from cooling the translational motion, the buffer gas is then also required to cool internal degrees of freedom via inelastic collisions. Furthermore, buffer gas may be a useful tool to quench excited vibrational levels when they get populated during laser cooling due to the nondiagonal Franck-Condon factors. This could circumvent the need for additional repumping lasers. In a similar scheme, rotational buffer gas cooling was performed during sympathetic translational cooling of MgH^+ [48].

In a recent paper we calculated cross sections and rate coefficients for C_2^- -He rotationally inelastic collisions, treating the anion as a rigid rotor [49]. The rates for rotational excitation and quenching were found to be in line with those for similar ionic molecules interacting with helium [46]. Simulations of cooling rotational motion at typical helium pressures in ion traps showed thermalization to Boltzmann populations occurred within tenths of seconds. Very recently we have extended this work and also modeled the rotational cooling of C_2^- with neon and argon [50]. It was found that thermalization times of C_2^- with He and Ne were fairly similar but cooling was significantly faster with Ar. This is due to the increased interaction strength between C_2^- and the larger atoms which increased as expected in the series He < Ne < Ar.

In this work we present results for the quenching of internal vibrational motion of C_2^- in its ground $^2\Sigma_g^+$ electronic state in collisions with the noble-gas atoms helium, neon, and argon. A simplified view of the relevant vibrational levels involved in these processes is shown specifically in Fig. 1. We know, however, that no quantitative rate coefficients for vibrational relaxation are available to date. As C_2^- has no oscillating dipole, the vibrational levels are long lived with the ground

electronic state's $v = 2$ levels persisting for over 5 s [24] and so collisions are the only viable means of quenching these states efficiently. The rate coefficients of C_2^- vibrational quenching with helium may also prove useful in future astronomical studies, should the anion be detected in an interstellar environment where excited vibrational states are important for observation, as in the circumstellar envelope around carbon-rich stars where helium atoms are also abundant.

The paper is organized as follows. In the next section we discuss the potential energy curve (PEC) and vibrational levels of the isolated C_2^- in its ground electronic $^2\Sigma_g^+$ state. We further calculate the dipole moment of the $^{12}C^{13}C^-$ isotopologue and discuss its value. In Sec. III we provide details of *ab initio* calculations for the three-dimensional (3D) potential energy surfaces (PES) and fitting of the surfaces to a functional form. This section also contains details of the vibrationally averaged matrix elements required for scattering calculations. Details of the close-coupled scattering calculations are given in Sec. IV. Cross sections and corresponding rates for rotationally and vibrationally inelastic collisions are presented in Sec. V. We present conclusions in Sec. VI.

II. $C_2^- (^2\Sigma_g^+)$ POTENTIAL ENERGY CURVE AND $^{12}C^{13}C^-$ DIPOLE MOMENT

As recently discussed by Gulania *et al.* [36], the electronic structure of the C_2 molecule is notoriously difficult to calculate accurately due to many low-lying electronic states giving rise to a multireference character of the *ab initio* description of its ground electronic state. For the C_2^- anion considered here, the situation is not so severe but the presence of a close-lying $A^2\Pi_u$ state (4000 cm^{-1} above the ground $^2\Sigma_g^+$ state, see Fig. 1) still makes electronic structure calculations challenging.

The PEC of C_2^- in its ground $^2\Sigma_g^+$ state was calculated from the 3D potential energy surfaces (see next section) with the noble-gas atom at $R = 25 \text{ \AA}$. The LEVEL program [52] was used to obtain the vibrational energies and wave functions for the C_2^- molecule. *Ab initio* PEC points were used as input, interpolated using a cubic spline and extrapolated to r values below and above our range using functions implemented in LEVEL. The relative energies of the first three vibrational levels along with the rotational constants for each state are shown in Table I and compared with previously published calculated theoretical and experimental values. Table I also compares the values obtained for the multiconfiguration-self-consistent-field (MCSCF) method which was used for the C_2^- -He PES and the coupled-cluster singles-doubles perturbative triples (CCSD-T) method which was used for C_2^- -Ne/Ar (see next section). While we do not achieve spectroscopic accuracy with our PEC, the relative energy spacings are sufficiently realistic for computing the vibrational quenching rates of interest here at a reliable level. The results obtained for CCSD-T are closer in agreement to experiment than those for the MCSCF method but the differences will have a minimal impact on the computed inelastic rate coefficients obtained from our scattering calculations of interest here. The PEC fit using LEVEL to the CCSD-T calculations and vibrational wave functions for $v = 1, 2$, and 3 are provided in the Supplemental Material [53].

TABLE I. Comparison of vibrational energies and rotational constants with previous theoretical and experimental values. Literature values calculated from Dunham parameters provided. Units of cm⁻¹.

		Relative energy	B _v
ν ₀	MCSCF	0	1.7455
	CCSD-T	0	1.7356
	Calc. [8]	0	1.7358
	Expt. [19]	0	1.7384
ν ₁	MCSCF	1805	1.7419
	CCSD-T	1776	1.7222
	Calc. [8]	1759	1.7197
	Expt. [19]	1757	1.7220
ν ₂	MCSCF	3633	1.7190
	CCSD-T	3561	1.7126
	Calc. [8]	3494	1.7035
	Expt. [19]	3492	1.7062

As discussed above, the C₂ molecule has been detected in various astronomical settings [37–40] but searches for the C₂⁻ anion focusing on electronic transitions have so far not been conclusive [42–44]. Franck-Condon factors and Einstein A coefficients for these transitions have been calculated by Shi *et al.* [8]. Another possible detection method, at least in principle, is the rotational transitions of the ¹³C¹²C⁻ isotopologue [34]. The rotational constants for this isotopologue were accurately calculated by Šedivcová and Špirko [34]. Here we use our PEC to assess the dipole moment of ¹³C¹²C⁻ and Einstein A coefficients for rotational transitions.

The dipole moment of a charged homonuclear diatomic with different isotopes arises due to the difference in the center of mass and center of charge. An expression for the dipole moment of HD⁺ was derived by Bunker [54] and Ellison [55] as

$$\mu(v', v) = -[(m_a - m_b)/2m_T]e\langle v'|r|v\rangle, \quad (1)$$

where m_a and m_b are the masses of each nucleus and $m_T = m_a + m_b$. Using LEVEL, the matrix element of the vibrational coordinate r for ¹³C¹²C⁻ for the $v' = v = 0$ ground vibrational state was calculated as 1.27 Å, close to the equilibrium geometry of C₂⁻ of $r_{eq} = 1.2689$ Å [8]. Using the masses for ¹³C¹²C⁻ in Eq. (1) gives $\mu(0, 0) = 0.12$ D. This compares to 0.87 D in HD⁺ [54]. For pure rotational transitions, the Einstein coefficient for spontaneous dipole transitions is given as [46]

$$A_{k \rightarrow i} = \frac{2}{3} \frac{\omega_{k \rightarrow i}^3}{\epsilon_0 c^3 h} \mu_0^2 \frac{j_k}{(2j_k + 1)}, \quad (2)$$

where $\omega_{i \rightarrow k} \approx 2B_0(j_i + 1)$ is the transition's angular frequency. In Table II the Einstein A coefficients computed using Eq. (2) for ¹²C¹³C⁻ (treated as pseudosinglet), HD⁺ and C₂H⁻ are compared for the first few rotational levels. The Einstein A coefficients for ¹²C¹³C⁻ are orders of magnitude smaller than for HD⁺ and C₂H⁻ and other molecular ions [46]. The combination of very small rotational emission coefficients coupled with the isotope ratio for ¹³C/¹²C of 0.01 suggests that detecting C₂⁻ via the rotational transitions of the ¹²C¹³C⁻ isotopologue would be very difficult.

TABLE II. Computed Einstein spontaneous emission coefficients $A_{j \rightarrow j'}$ for ¹²C¹³C⁻ ($B_0 = 1.67152$ cm⁻¹ [34], $\mu = 0.12$ D), HD⁺ ($B_e = 22.5$ cm⁻¹ [56]), $\mu = 0.87$ D [54], and C₂H⁻ ($B_e = 1.389$ cm⁻¹ [57], $\mu = 3.09$ D [58]). All quantities in units of s⁻¹.

Transition	¹² C ¹³ C ⁻	HD ⁺	C ₂ H ⁻
1 → 0	5.6×10^{-8}	7.2×10^{-3}	2.14×10^{-5}
2 → 1	5.4×10^{-7}	6.9×10^{-2}	2.05×10^{-4}
3 → 2	1.9×10^{-6}	2.5×10^{-1}	7.43×10^{-4}
4 → 3	4.8×10^{-6}	6.0×10^{-1}	1.83×10^{-3}
5 → 4	9.6×10^{-6}	1.2×10^0	3.65×10^{-3}

III. C₂⁻-He/Ne/Ar 3D POTENTIAL ENERGY SURFACES AND VIBRATIONALLY AVERAGED MATRIX ELEMENTS

The interaction energies between C₂⁻ in its ground ²Σ_g⁺ electronic state with He, Ne, and Ar atoms were calculated using *ab initio* methods implemented in the MOLPRO suite of codes [59,60]. Geometries were defined on a Jacobi grid with R (the distance from the center of mass of C₂⁻ to the atom) ranging from 2.6 to 25 Å and θ (the angle between R and the C₂⁻ internuclear axis r) from 0 to 90° in 10° intervals. Five values of the C-C bond length for each system between $r = 1.10$ – 1.35 Å were used including the equilibrium value of $r_{eq} = 1.269$ Å. This is sufficient to cover the vibrational levels of interest in this study. Interaction potential energies between C₂⁻ and the noble-gas atoms were determined by subtracting the asymptotic energies for each bond length.

For C₂⁻-He, energies were calculated using the 2 × 2 multiconfigurational self-consistent field (MCSCF) method [61,62] with 10 occupied orbitals and 4 closed orbitals followed by a 2-state multireference configuration interaction (MRCI) [63] calculation. An aug-cc-pVQZ basis [64] was used on each carbon center and an aug-cc-pV5Z basis on the helium atom. For the C₂⁻-Ne and Ar systems, convergence problems were encountered for the MCSCF approach and so energies were instead calculated using the partially spin restricted coupled-cluster singles-doubles perturbative triples (RCCSD-T) method for open shell systems [65,66] with complete basis-set (CBS) extrapolation using the aug-cc-pVTZ, aug-cc-pVQZ, and aug-cc-pV5Z basis sets [67,68]. The same method for the case of C₂⁻-He provided results within a few wave numbers of the MCSCF approach. The basis-set-superposition-error (BSSE) was also accounted for at all calculated points using the counterpoise procedure [69].

The three-dimensional PESs were fit to an analytical form using the method of Werner, Follmeg, and Alexander [70,71] where the interaction energy is given as

$$V_{\text{int}}(R, r, \theta) = \sum_{n=0}^{N_r-1} \sum_{l=0}^{N_\theta-1} P_l(\cos \theta) A_{ln}(R) (r - r_{eq})^n, \quad (3)$$

where $N_r = 5$ and $N_\theta = 10$ are the number of bond lengths r and angles θ in our *ab initio* grid, $P_l(\cos \theta)$ are the Legendre polynomials where due to the symmetry around $\theta = 90^\circ$ only even values of l are used, and $r_{eq} = 1.2689$ Å is the equilibrium bond length of C₂⁻. For each bond length r_m and angle

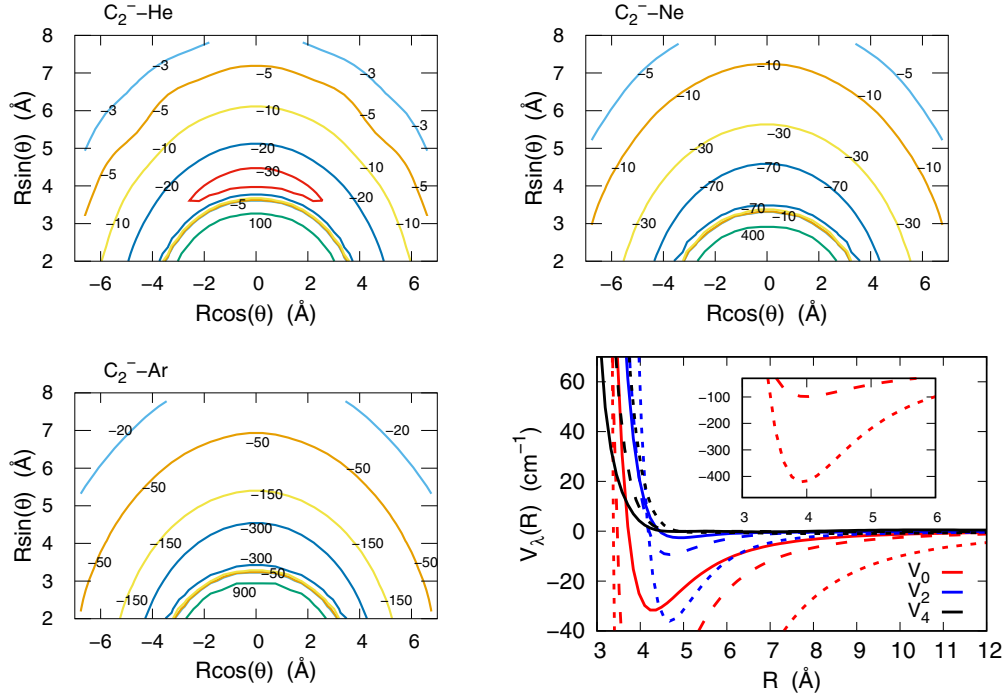


FIG. 2. Contour plots of $C_2^-(^2\Sigma_g^+)$ -He (top left), Ne (top right), and Ar (bottom left) vibrationally averaged matrix elements $V_{0,0}(R, \theta)$ projected onto Cartesian coordinates. Energies in cm^{-1} . Bottom right is expansion of matrix elements in V_λ coefficients for $V_{0,0}$ for He (solid lines), Ne (long dashed lines), and Ar (short dashed lines). V_0 in red (light gray), V_2 in blue (darker gray), and V_4 in black.

θ_k , one-dimensional cuts of the PESs $V_{\text{int}}(R, r_m, \theta_k)$ were fit to

$$B_{km}(R) = \exp(-a_{km}R) \left[\sum_{i=0}^{i_{\text{max}}} b_{km}^{(i)} R^i \right] - \frac{1}{2} [1 + \tanh(R)] \left[\sum_{j=j_{\text{min}}}^{j_{\text{max}}} c_{km}^j R^{-j} \right], \quad (4)$$

where the first terms account for the short-range part of the potential and the second part for the long-range terms combined using the $\frac{1}{2}[1 + \tanh(R)]$ switching function. For each r_m and θ_k , Eq. (4) was least-squares fit to the *ab initio* data (around 40 R points) using $i_{\text{max}} = 2$, $j_{\text{min}} = 4$, and $j_{\text{max}} = 10$ for eight variable parameters. The average root-mean-square error (RMSE) for each fit was 0.5 cm^{-1} for C_2^- -He and Ne, rising to 1 cm^{-1} for Ar. From the one-dimensional (1D) potential fits $B_{km}(R)$, the radial coefficients $A_{lm}(R)$ can be determined from the matrix product $\mathbf{A}(R) = \mathbf{P}^{-1}\mathbf{B}(R)\mathbf{S}^{-1}$ where the matrix elements of \mathbf{P} and \mathbf{S} are given as $P_{kl} = P_l(\cos \theta_k)$ and $S_{nm} = (r_m - r_{eq})^n$, respectively. The analytical representation of the PES [Eq. (3)] gives a reasonable representation of the *ab initio* interaction energies. An RMSE of 1.5 cm^{-1} for $V < 200 \text{ cm}^{-1}$ and 0.9 cm^{-1} for $V < 0 \text{ cm}^{-1}$ was obtained for the C_2^- -He system while for the C_2^- -Ne and Ar systems, RMSEs of 0.5 and 3.5 cm^{-1} , respectively, for $V < 1500 \text{ cm}^{-1}$ were obtained.

The scattering calculations described in the next section require the interaction potential to be averaged over the vibrational states of C_2^- as

$$V_{v,v'}(R, \theta) = \langle \chi_v(r) | V_{\text{int}}(R, r, \theta) | \chi_{v'}(r) \rangle. \quad (5)$$

Figure 2 shows the diagonal terms $V_{0,0}(R, \theta)$ for each system. As expected for a molecule with a strong bond, the contour plots of the $V_{0,0}(R, \theta)$ for each system are very similar to our earlier rigid-rotor (RR) PESs which were obtained without the vibrational averaging (and a different *ab initio* method for C_2^- -He) [49,50]. The minimum values of $V_{0,0}$ for each system occur at perpendicular geometries and are around -30 cm^{-1} at 4.5 \AA for He, -110 cm^{-1} at 3.7 \AA for Ne, and -490 cm^{-1} at 3.7 \AA for Ar. Each system's PES has a fairly similar appearance with the well depth being the main difference which increases as expected from He to Ne to Ar due to the increasing number of electrons on the atoms and on the much larger dipole polarizability that dominates the long-range attractive terms with a value of $1.383 a_0^3$ for He, $2.660 a_0^3$ for Ne, and $11.070 a_0^3$ for Ar [72].

The off-diagonal $V_{0,1}(R, \theta)$ terms which directly drive vibrationally inelastic $v = 1$ to $v = 0$ transitions are shown in Fig. 3. At short distances the coupling terms are repulsive, becoming negligible quickly at longer distances, as is the case for many other atom-diatom systems. It can be seen that for C_2^- interacting with He and Ne the $V_{0,1}(R, \theta)$ plots are quite similar but the interaction with Ar is more repulsive. This suggests collisions with Ar have larger vibrational cross sections as will be shown below. The $V_{0,2}(R, \theta)$ and $V_{1,2}(R, \theta)$ matrix elements have a similar appearance to those of $V_{0,1}(R, \theta)$.

The close-coupling scattering calculations discussed in the next section require the vibrationally averaged matrix elements in the form of a multipole expansion as

$$V_{v,v'}(R, \theta) = \sum_{\lambda}^{\lambda_{\text{max}}} V_{v,v'}^{\lambda}(R) P_{\lambda}(\cos \theta), \quad (6)$$

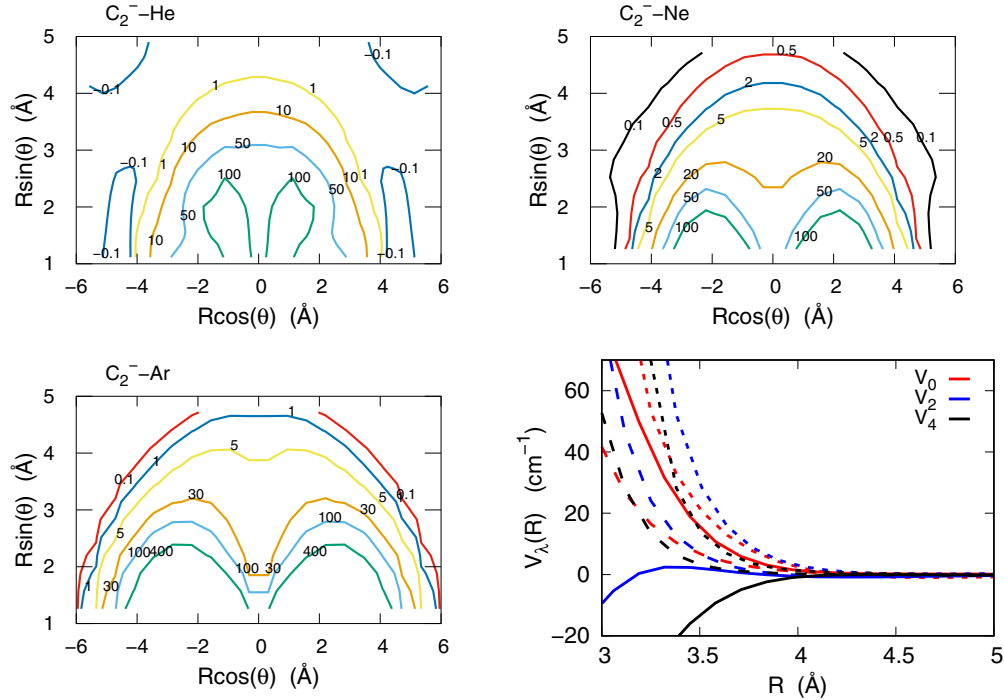


FIG. 3. Contour plots of $C_2^-(^2\Sigma_g^+)$ -He (top left), Ne (top right), and Ar (bottom left) vibrationally averaged matrix elements $V_{0,1}(R, \theta)$ projected onto Cartesian coordinates. Energies in cm^{-1} . Bottom right is expansion of matrix elements in V_λ coefficients for $V_{0,1}$ for He (solid lines), Ne (long dashed lines), and Ar (short dashed lines). V_0 in red (light gray), V_2 in blue (darker gray), and V_4 in black.

where again due C_2^- being a homonuclear diatomic, only even λ terms are required. The bottom right panels of Figs. 2 and 3 compare the $V_{0,0/1}^\lambda(R)$ coefficients for the most important $\lambda = 0, 2$, and 4 coefficients. As with the contour plots of Fig. 2, the $V_{0,0}^\lambda(R)$ expansion coefficients are very similar to their rigid-rotor counterparts [49,50]. This means that rotationally inelastic collisions using the vibrationally averaged multipole expansion will have very similar values to those obtained using a rigid-rotor treatment as will be shown in Sec. V A. As for other atom-diatom systems, $V_{v,v}^\lambda(R)$ for other vibrational states v are very similar to those for $V_{0,0}^\lambda(R)$ and thus rotations and vibrations can essentially be considered separately.

For the off-diagonal expansion coefficients $V_{0,1}^\lambda$, all terms quickly approach zero as R is increased. For all three systems the $V_{0,1}^0(R)$ coefficients are steeply repulsive as R decreases. For the C_2^- -He system, however, the $V_{0,1}^2(R)$ and $V_{0,1}^4(R)$ terms are attractive in contrast to Ne and Ar which are also repulsive. As expected from the contour plots, the $V_{0,1}^\lambda(R)$ terms are the most repulsive for the C_2^- -Ar interaction.

The PES functions and vibrationally averaged matrix elements used for each system are provided in the Supplemental Material [53].

IV. QUANTUM SCATTERING CALCULATIONS

Quantum scattering calculations were carried out using the coupled channel (CC) method to solve the Schrödinger equation for scattering of an atom with a diatomic molecule as implemented in our in-house code ASPIN [73]. The method has been described in detail before [73,74] and only a brief

summary will be given here, with equations given in atomic units. For a given total angular momentum $\mathbf{J} = \mathbf{l} + \mathbf{j}$ the scattering wave function is expanded as

$$\Psi^{JM}(R, r, \Theta) = \frac{1}{R} \sum_{v,j,l} f_{vlj}^J(R) \chi_{v,j}(r) \mathcal{Y}_{jl}^{JM}(\hat{\mathbf{R}}, \hat{\mathbf{r}}), \quad (7)$$

where l and j are the orbital and rotational angular momentum, respectively, $\mathcal{Y}_{jl}^{JM}(\hat{\mathbf{R}}, \hat{\mathbf{r}})$ are coupled-spherical harmonics for l and j which are eigenfunctions of J . $\chi_{v,j}(r)$ are the radial part of the rovibrational eigenfunctions of the molecule. The values of l and j are constrained, via Clebsch-Gordan coefficients, such that their resultant summation is compatible with the total angular momentum J [73,74]. $f_{vlj}^J(R)$ are the radial expansion functions which need to be determined. Substituting the expansion into the Schrödinger equation with the Hamiltonian for atom-diatom scattering [73,74] leads to the CC equations for each J :

$$\left(\frac{d^2}{dR^2} + \mathbf{K}^2 - \mathbf{V} - \frac{\mathbf{l}^2}{R^2} \right) \mathbf{f}^J = 0. \quad (8)$$

Here, each element of $\mathbf{K} = \delta_{i,j} 2\mu(E - \epsilon_i)$ (where ϵ_i is the channel asymptotic energy), μ is the reduced mass of the system, $\mathbf{V} = 2\mu\mathbf{U}$ is the interaction potential matrix between channels, and \mathbf{l}^2 is the matrix of orbital angular momentum. For the rovibrational scattering calculations of interest here, the matrix elements \mathbf{U} are given explicitly as

$$\langle vjlJ | \mathbf{U} | v'j'l'J \rangle = \int_0^\infty dr \int d\hat{\mathbf{r}} \int d\hat{\mathbf{R}} \chi_{v,j}(r) \mathcal{Y}_{jl}^{JM}(\hat{\mathbf{R}}, \hat{\mathbf{r}})^* \times |V(R, r, \theta)| \chi_{v',j'}(r) \mathcal{Y}_{j'l'}^{JM}(\hat{\mathbf{R}}, \hat{\mathbf{r}}). \quad (9)$$

As the intermolecular potential $V(R, r, \theta)$ is expressed as in Eq. (6), Eq. (9) can be written as

$$\langle v j l J | V | v' j' l' J \rangle = \sum_{\lambda=0}^{\infty} V_{v, v'}^{\lambda}(R) f_{\lambda j l j' l'}^J, \quad (10)$$

where the $f_{\lambda j l j' l'}^J$ terms are the Percival-Seaton coefficients

$$f_{\lambda j l j' l'}^J = \int d\hat{\mathbf{r}} \int d\hat{\mathbf{R}} \mathcal{Y}_{j l}^{JM}(\hat{\mathbf{R}}, \hat{\mathbf{r}}) P_{\lambda}(\cos \theta) \mathcal{Y}_{j' l'}^{JM}(\hat{\mathbf{R}}, \hat{\mathbf{r}}), \quad (11)$$

for which analytical forms are known [73]. Equation (10) also makes use of the widely known approximation

$$V_{v, v'}^{\lambda}(R) \approx V_{v j v' j'}^{\lambda}(R), \quad (12)$$

for all j such that the effect of rotation on the vibrational matrix elements is ignored.

The CC equations are propagated outward from the classically forbidden region to a sufficient distance where the scattering matrix \mathbf{S} can be obtained. The rovibrational state-changing cross sections are obtained as

$$\begin{aligned} \sigma_{v j \rightarrow v' j'} &= \frac{\pi}{(2j+1)k_{vj}^2} \sum_J (2J+1) \\ &\times \sum_{l, l'} |\delta_{v l j, v' l' j'} - S_{v l j, v' l' j'}^J|^2. \end{aligned} \quad (13)$$

In all scattering calculations the C_2^- anion was treated as pseudosinglet ($^1\Sigma$) and the effects of spin-rotation coupling were ignored. In our previous work on this system it was shown that a pseudosinglet treatment of the rotational state-changing collisions resulted in essentially the same results as the explicit doublet calculation when the relevant cross sections were summed [49]. This approximation reduces the computational cost of the scattering calculations without significantly affecting the size of the cross sections and thus the main conclusions.

To converge the CC equations, a rotational basis set was used which included up to $j = 20$ rotational functions for each vibrational state. The CC equations were propagated between 1.7 and 100.0 Å using the log-derivative propagator [75] up to 60 Å and the variable-phase method at larger distances [76]. The potential energy was interpolated between calculated $V_{v, v'}^{\lambda}(R)$ values using a cubic spline. For $R < 2.6$ Å the $V_{v, v'}^{\lambda}(R)$ were extrapolated as $\frac{a_{\lambda}}{R} + b_{\lambda} R$ while for $R > 20$ Å the $\lambda = 0$ terms were extrapolated as $\frac{c}{R^4} + \frac{d}{R^6}$. As our *ab initio* calculated interaction energies were computed to $R = 25$ Å where the interaction energy is negligible for the temperature of interest here, the extrapolated form has also a negligible effect on cross sections [49].

A number of parameters of the calculation were checked for convergence. The number of λ terms from Eq. (6) was checked for both rotationally and vibrationally inelastic collisions. For the former, calculations were converged to better than 1% using only three terms (up to $\lambda = 4$). For vibrationally inelastic collisions the convergence with increasing λ is less precise: with five λ terms convergence to tens of percent is achieved for He and Ne. For Ar convergence to within about a factor of 2 is achieved. This is due to the very small cross sections for these processes which makes obtaining precise

and stable values more difficult to achieve. For production calculations, nine λ terms were included for each $V_{v, v'}(R)$.

The effect of the PES fitting function was also checked. For the C_2^- -He system a PES fit was carried out using only three r terms with $r = 1.10, 1.2689, \text{ and } 1.35$ Å. This change resulted in tens of percent changes to the vibrationally inelastic cross sections. The fitting function (3) does not extrapolate well and this change from a fifth- to third-order polynomial fit for r has a drastic effect on the variation in potential energy with r for values below and above the range used for fitting. Despite this, the vibrationally inelastic cross sections remained reasonably consistent and thus our r range is sufficient to obtain cross sections which are to the correct order of magnitude, sufficient to assess rates for vibrational quenching of C_2^- with each of the noble-gas atoms.

As a final check of our calculation parameters, the effect of the vibrational basis set was also considered. In all calculations we used the vibrational energies and rotational constants obtained from calculations using LEVEL and employing our own C_2^- PEC as discussed in Sec. II. It was found that for $\nu = 1$ and 2, which are the states of interest here (see next section), it was sufficient to only include these states. Including the $\nu = 3$ state had a negligible effect on the $\nu = 1$ and 2 quenching cross sections.

Scattering calculations were carried out for collision energies between 1 and 1000 cm^{-1} using steps of 0.1 cm^{-1} for energies up to 100 cm^{-1} , 0.2 cm^{-1} for 100–200 cm^{-1} , 1.0 cm^{-1} for 200–300 cm^{-1} , 2 cm^{-1} for 300–700 cm^{-1} , and 4 cm^{-1} for 700–1000 cm^{-1} . This fine energy grid was used to ensure that important features such as resonances appearing in the cross sections were accounted for and their contributions correctly included when the corresponding rates were calculated. At low collision energies, such resonances will be very sensitive to the details of the PES (see below). The number of partial waves was increased with increasing energy up to $J = 100$ for the highest energies considered.

V. RESULTS

A. Rotationally inelastic cross sections

Rotationally inelastic cross sections for C_2^- -He collisions can be used to compare our present calculations with those of our previous work which considered rotationally inelastic collisions treating the anion as a rigid rotor [49]. Figure 4 shows rotationally inelastic cross sections for selected $j \rightarrow j'$ transitions for both excitation and deexcitation processes. The figure compares using a vibrationally averaged (VA) PES, that is, only $V_{0,0}^{\lambda}$ coefficients from Eq. (6), to using the *ab initio* PES to carry out RR calculations at $r = r_{eq}$ and our previous RR calculations which used the CCSD(T) method to compute interaction energies [49]. The RR calculations do not carry out the VA procedure of Eq. (5) and instead expansion coefficients in Eq. (6) are obtained only for $r = r_{eq}$.

The differences between the VA and RR cross sections obtained using the present PES are small, as is expected since the $\nu = 0$ vibrational wave function is strongly peaked around $r = r_{eq}$. This behavior was also found for H_2^+ -He collisions [77] and justifies our previous treatment of the molecule as a rigid rotor. From Fig. 4 it can also be seen that the rotationally

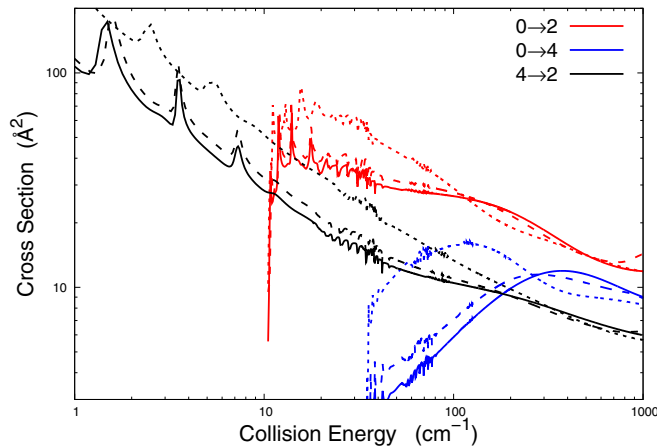


FIG. 4. Rotationally inelastic cross sections computed using vibrationally averaged method (solid lines), using a RR approach with the current PES for $r = r_{eq}$ (long-dashed lines) and those of our previous RR PES (short-dashed lines) [49].

inelastic collisions using our PES are in quite good agreement with our previous work as anticipated from the similarity of the multipolar expansion coefficients in Fig. 2 to our previous work [49]. The profiles of the cross sections with energy variation are similar and resonances appear at similar energies. Cross sections only differ by tens of percent and these differences will have a negligible effect on the corresponding rotationally inelastic rates.

Rotationally inelastic collisions can also be used to assess the effect of vibrational state on rotationally inelastic collision. Figure 5 shows selected rotationally inelastic vibrationally elastic cross sections for C_2^- -He for the $\nu = 0, 1$, and 2 vibrational states. As mentioned in Sec. III, the $V_{v,v'}^\lambda$ coefficients for $\nu = \nu'$ are very similar resulting in very similar rotationally inelastic cross sections for a given vibrational state. This insensitivity of rotationally inelastic cross sections to vibrational state has been seen for many other molecules undergoing collisions with He [71,78–81] and Ar [82,83] and

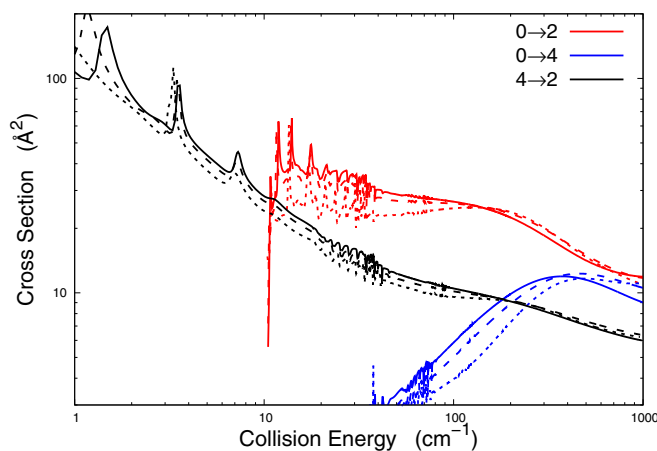


FIG. 5. Rotationally inelastic vibrationally elastic cross sections for C_2^- -He collisions computed for $\nu = 0$ (solid lines), $\nu = 1$ (long-dashed lines), and $\nu = 2$ (short-dashed lines).

is a consequence of the small off-diagonal vibrational matrix elements of the PES compared to diagonal ones in Eq. (6).

The results shown in this section for C_2^- -He collisions have demonstrated that rotational and vibrational collisions can essentially be considered separately. We have recently compared rotationally inelastic thermal quenching cross sections, rates, and times for C_2^- in collisions with He, Ne, and Ar and we refer the reader to this work for further details of this process [50].

The 2D RR PES functions and Legendre expansions for each system are provided in the Supplemental Material [53].

B. Vibrationally inelastic cross sections

As discussed in the Introduction, vibrationally inelastic collisions of C_2^- with helium buffer gas have been suggested to cool the molecules to their $\nu = 0$ vibrational ground state. As shown in Fig. 1, the ground vibrational state of the $A^2\Pi_u$ electronic state is lower in energy than the $\nu = 3$ state of the $X^2\Sigma_g^+$ ground electronic state. It therefore follows that the vibrational states above $\nu = 2$ in $X^2\Sigma_g^+$ can decay to the $A^2\Pi_u$ state by dipole allowed transitions which in turn decay into the $\nu = 2$ and below vibrational states of $X^2\Sigma_g^+$ [24]. As a consequence, we only consider here collisional quenching of the long-lived $\nu = 1$ and 2 vibrational states of C_2^- in its ground $X^2\Sigma_g^+$ electronic state.

From Fig. 1 it can also be seen that the $\nu = 2$ vibrational level of the $X^2\Sigma_g^+$ state is close in energy to the $\nu' = 0$ state of the excited electronic $A^2\Pi_u$ state with an energy difference relative to the bottom of the $X^2\Sigma_g^+$ PEC of $\approx(4837-4380) = 457 \text{ cm}^{-1}$ [8]. This close energy spacing could cause the $\nu' = 0$ state to perturb the $\nu = 2$ state through nonadiabatic effects during collisions. This was also a concern for the neutral C_2 -He system where for the isolated molecule the energy difference between the ground $X^2\Sigma_g^+$ and excited $a^3\Pi_u$ state is only around 700 cm^{-1} [36]. For C_2 -He rigid-rotor rotationally inelastic scattering, Naja *et al.* [84] found that at the $C_2 X^2\Sigma_g^+$ equilibrium geometry, the energy separation between the $X^2\Sigma_g^+$ and $a^3\Pi_u$ states is 2000 cm^{-1} which remained at this value even with the approach of the He atom. In this case, electronic state coupling could be ignored. When vibrations are involved, the situation is more complicated as states can be coupled via the r vibrational coordinate. This is the case for the H^+ -CO and H^+ -CN systems which have been studied by Kumar *et al.* [85–87]. For these systems the naked positive charge of the proton has a strong perturbing effect and can couple the molecule's electronic states. The strength of the coupling can be calculated as $\{\psi_i^\alpha | \frac{\partial^n}{\partial Q^n} | \psi_j^\alpha\}$ where $\psi_{i/j}^\alpha$ are the electronic wave functions and the operator is the first ($n = 1$) or second ($n = 2$) derivative with respect to the nuclear coordinate Q ($=r$ for diatomics) [85–87]. The coupling matrix was used to carry out H^+ -CO scattering calculations by constructing diabatic PESs for two electronic states allowing a computation of elastic, vibrationally inelastic, and charge transfer probabilities [88]. The present systems involve the rather weak interaction of an anion with closed-shell noble gases so that the gradient couplings between the relevant electronic states should be smaller than in the case of the naked proton as a partner as in the case of the work of

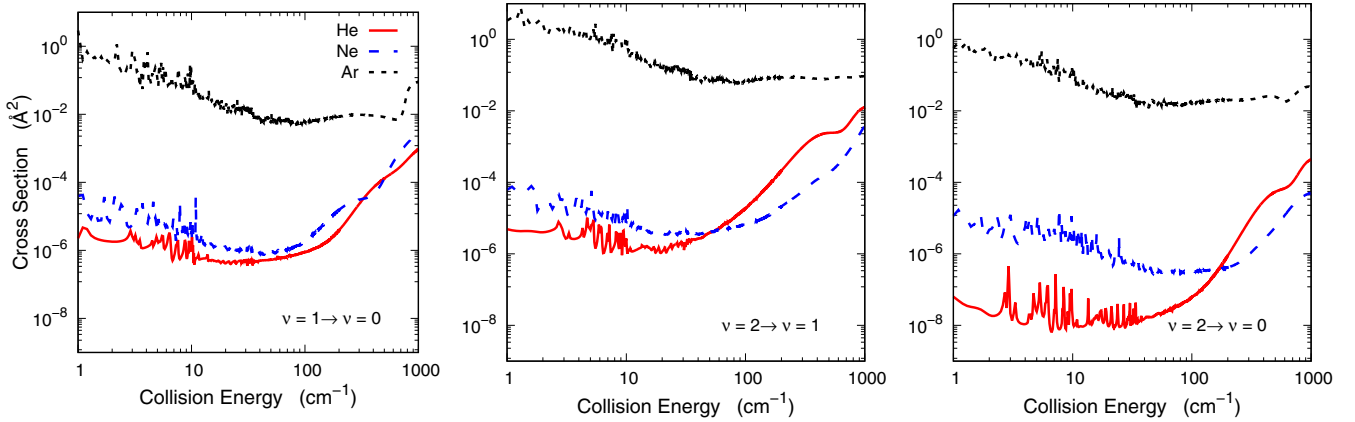


FIG. 6. Comparison of vibrationally inelastic rotationally elastic cross sections for $\nu = 1 \rightarrow \nu = 0$ (left panel), $\nu = 2 \rightarrow \nu = 1$ (center panel), and $\nu = 2 \rightarrow \nu = 0$ (right panel) transitions for collisions of C_2^- with He, Ne, and Ar atoms.

Kumar *et al.* Kendrick also recently studied $HD + H$ reactive scattering for excited vibrational states (those energetically above and below a conical intersection on the PES) using two coupled diabatic PESs and found significant differences to the adiabatic approach [89]. Kendrick has also given a detailed approach for nonadiabatic reactive scattering [90]. To apply these approaches to the C_2^- -He/Ne/Ar systems would involve using an *ab initio* method such as complete-active-space self-consistent-field (CASSCF) or MRCI to obtain the ground and electronically excited PESs and assessing them as a function of R , r , and θ coordinates. The coupling matrices could be calculated as described above and diabatic states constructed. This is somewhat beyond the scope of this work but whether nonadiabatic effects would alter quenching rates is an interesting question and would depend on the magnitude of the coupling compared to inaccuracies in the adiabatic PES.

Figure 6 compares vibrationally inelastic rotationally elastic (for $j = j' = 0$) cross sections for the deexcitation $\nu = 1 \rightarrow \nu = 0$, $\nu = 2 \rightarrow \nu = 1$, and $\nu = 2 \rightarrow \nu = 0$ transitions for C_2^- colliding with He, Ne, and Ar atoms. At low collision energies between 0.1 to around 60 cm^{-1} the cross sections for He and Ne are very small, orders of magnitude less than rotationally inelastic cross sections. The $\nu = 2 \rightarrow \nu = 0$ process is an order of magnitude smaller than the $\Delta\nu = -1$ transitions as is common for cross sections for larger energy differences between states. The cross sections show resonances at lower collision energies. These are likely due to shape or Feshbach resonances. As is well established, the location and widths of resonances in the scattering cross sections at low collision energies are very sensitive to the details of the PES [91,92] and there is currently an effort to obtain reliable information about scattering observables, particularly for ultracold regimes, such as the statistical method of Morita *et al.* [93]. As we are primarily interested in assessing the rates for vibrational quenching for temperatures of 5–100 K, the fine details of the low-energy resonances are less important since the Boltzmann average over the cross sections in this temperature range is likely to be far less sensitive to the details of the PES.

For He and Ne, in all three processes the cross sections begin to increase in magnitude above 100 cm^{-1} . This is a well-known trend for vibrationally inelastic collisions [71,79–81]. This trend is a consequence of the PES in Fig. 2 and

the vibrational matrix elements in Fig. 3: the off-diagonal matrix elements which couple different vibrational states are only significant at small- R values where the PES is repulsive. The incoming atom thus requires a higher kinetic energy to allow the scattering wave function to become significant in this region and therefore facilitate vibrational transitions. The C_2^- -Ar cross sections are more constant in value at the higher energies, however, a feature which is likely to be due to the more attractive potential exhibited by this system, which then allows the scattering wave function to build up more significantly in the repulsive region, thereby allowing the occurrence of larger inelastic vibrational cross sections.

Comparing the cross sections for collisions of C_2^- with He, Ne, and Ar, some general trends are apparent. The cross sections for Ar are orders of magnitude larger than those of He and Ne which are broadly similar in size. This can be rationalized by comparing the interactions shown in Figs. 2 and 3. The well depth of the $V_{0,0}(R, \theta)$ elements for the C_2^- -Ar is far larger than for He and Ne. This stronger interaction allows the incoming scattering wave function to build up more in the repulsive region where the off-diagonal $V_{0,1}(R, \theta)$ are significant, as opposed to He and Ne, for which the coupling potentials are much smaller. These matrix elements are therefore larger for Ar, thus giving rise to larger vibrationally inelastic cross sections in comparison with those from the lighter noble gases.

C. Vibrationally inelastic rates

The computed inelastic cross sections of the previous section can be used to obtain the corresponding thermal rate constants $k_{\nu \rightarrow \nu'}(T)$, which can be evaluated as the convolution of the computed inelastic cross sections over a Boltzmann distribution of the relative collision energies of the interacting partners as

$$k_{\nu \rightarrow \nu'}(T) = \left(\frac{8}{\pi \mu k_B^3 T^3} \right)^{1/2} \int_0^\infty E_c \sigma_{\nu \rightarrow \nu'}(E_c) e^{-E_c/k_B T} dE_c, \quad (14)$$

where $E_c = \mu v^2/2$ is the kinetic energy.

As discussed in the Introduction, studies on laser cooling of C_2^- have assumed the anion to be initially cooled to tens of

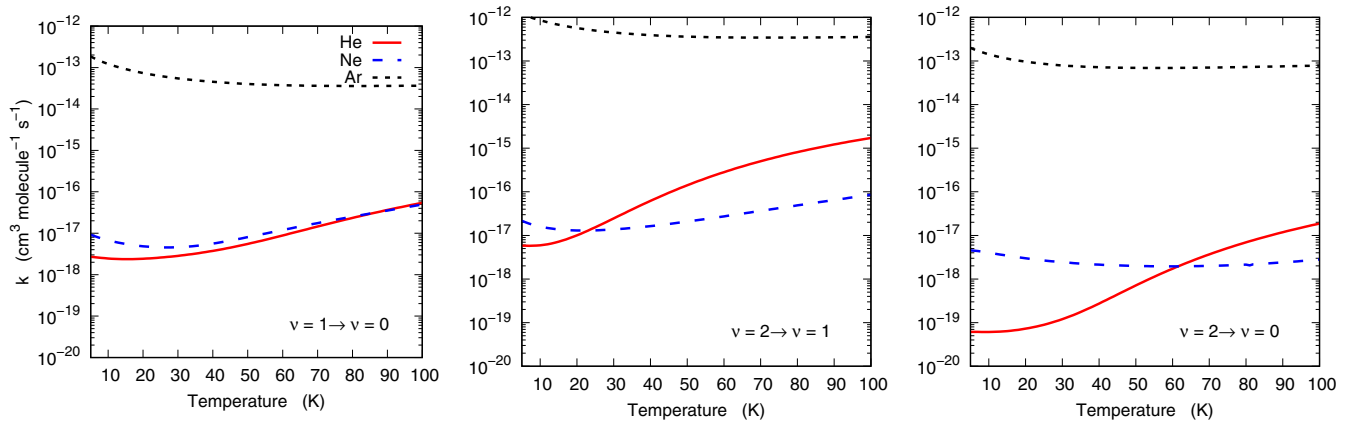


FIG. 7. Comparison of vibrational rate constants $k_{v,j \rightarrow v',j'}(T)$ for $v = 1 \rightarrow v = 0$ (left panel), $v = 2 \rightarrow v = 1$ (center panel), and $v = 2 \rightarrow v = 0$ (right panel) transitions for collisions of C_2^- with He, Ne, and Ar atoms.

kelvin [6] and thus the rate constants were computed between 5 and 100 K in 1-K intervals. Figure 7 shows the rates for vibrationally inelastic rotationally elastic ($j = j' = 0$) transitions corresponding to the cross sections in Fig. 6. The rates for the vibrational deexcitation processes for He and Ne are quite similar, particularly for the $v = 1 \rightarrow v = 0$ transition. They increase with increasing temperature as expected from the discussion in Sec. VB but even at 100 K, are at least four orders of magnitude smaller than the rotational deexcitation rates [50]. For Ar, the rates are more constant and are consistently two or three orders of magnitude larger than those for He or Ne. The vibrational quenching rates show some variation with the largest $v = 2 \rightarrow v = 1$ rate about an order of magnitude larger than the $v = 1 \rightarrow v = 0$ and $v = 2 \rightarrow v = 0$ rates which themselves are quite similar at the higher temperatures considered.

The trends in rates on going from He to Ne to Ar in collisions with C_2^- are similar to what was found for rotationally inelastic collisions [50] where the stronger interaction with the Ar atom resulted in larger rates and faster thermalization times compared to He or Ne. The larger quenching rates for Ar compared with He and Ne were not easy to predict *a priori*. Kato, Bierbaum, and Leone measured quenching rates of N_2^+ in collisions with He, Ne, Ar, Xe, and Kr at 300 K and found quenching rates increased with the size of atom [94]. This suggests that the polarizability of the colliding atom plays an important role. Ferguson found a similar trend for vibrational quenching of O_2^+ with He, Ne, and Ar atoms at 300 K [95]. In contrast, Saidani *et al.* calculated quenching rates for CN with He and Ar over a wide range of temperatures and found that cross sections and rates for Ar were orders of magnitude lower than those for He [96]. However, ionic interactions are driven by different forces than those acting between neutrals, so it is not obvious how such a result relates to the present findings for an anion.

It is well known that, generally, vibrational quenching of molecules due to collisions is inefficient. Measurements of low-temperature rate constants for quenching of the $v = 1$ level include NH undergoing collisions with He where the

rates are of the order of $4 \times 10^{-15} \text{ cm}^3 \text{ s}^{-1}$ [101]. There are, however, systems for which collisions are efficient at quenching vibrational motion. The low-frequency stretching mode (100) in SrOH has been shown to be efficiently deexcited in collisions with He [102]. There is also the dramatic case of the $BaCl^+ + Ca$ system where laser-cooled Ca atoms have been shown to efficiently quench vibrational motion with rates similar to rotational transitions [100,103].

The rates and cross sections calculated here for C_2^- -He/Ne/Ar vibrationally inelastic transitions can be compared to other systems. Table III compares cross sections and rate constants (where available) calculated for various systems for $v = 1 \rightarrow v = 0$ transitions. As a simple comparison metric, Table III also compares the minimum of the interaction potential for each system V_{\min} . From the table it can be seen that cationic molecules have orders of magnitude larger vibrationally inelastic cross sections and rates compared with neutral systems. The strength of interaction between the molecule and colliding atom, parametrized here by V_{\min} , plays a role in the efficiency vibrational quenching as it will allow the scattering wave function to build up for geometries where the coupling matrix is large [Eq. (5)]. This has also been rationalized in terms of a statistical model [100] where the well depth and diatomic vibrational frequency contribute to the density of states of the complex which increases the lifetime of the complex and allows efficient quenching. Other factors play a role such as the mass of the colliding partners (compare the very low rates for CN-Ar collisions compared to CN-He despite the former having a lower well depth) and the long-range attraction [95]. Nevertheless, Table III shows that, in general, cations will have far larger vibrational quenching rates than neutral molecules. The low rates for C_2^- -He vibrational quenching are similar to those of neutrals as expected based on the relatively weak interaction. To be noted is the behavior of the vibrationally inelastic rates when Ar is taken as the partner gas: the size of the rates brings their values in the range of those for cations interacting with He, indicating quantitatively the special behavior of this noble gas as a partner for C_2^- anions in cold traps.

TABLE III. Comparison of vibrationally inelastic cross sections and rates for different systems. Well depth V_{\min} in cm^{-1} , cross sections $\sigma_{\nu=1 \rightarrow \nu'=0}$ in \AA^2 for scattering energy of 10 cm^{-1} . Temperatures in kelvin and rate constants $k_{\nu=1 \rightarrow \nu'=0}(T)$ in $\text{cm}^3 \text{ s}^{-1}$. The “asterisk” indicates the value was estimated from graph.

System	V_{\min}	$\sigma_{\nu=1 \rightarrow \nu'=0}$	Temperature	$k_{\nu=1 \rightarrow \nu'=0}(T)$	Reference
Cations					
$\text{H}_2^+ + \text{He}$	-2700	10^*			[77]
$\text{NO}^+ + \text{He}$	-195	1^*	100	$7 \times 10^{-14*}$	[97]
$\text{Mg}^+ + \text{He}$	< -100	80^*			[98]
$\text{CH}^+ + \text{He}$	-514	10^*			[99]
$\text{BaCl}^+ + \text{Ca}$	-7442		0.1	$1 \times 10^{-9*}$	[100]
Neutrals					
$\text{SiO} + \text{He}$	-27		200	$5 \times 10^{-18*}$	[71]
$\text{CO} + \text{He}$	-24	$1 \times 10^{-8*}$	300	1×10^{-17}	[78]
$\text{SO} + \text{He}$	-35	$5 \times 10^{-5*}$	300	$4 \times 10^{-17*}$	[79]
$\text{CS} + \text{He}$	-22		300	$1 \times 10^{-17*}$	[80]
$\text{SiS} + \text{He}$	-20		300	$4 \times 10^{-17*}$	[81]
$\text{HF} + \text{Ar}$	-159	$1 \times 10^{-6*}$	100	7×10^{-17}	[83]
$\text{CN} + \text{He}$	-20	$1 \times 10^{-10*}$	100	$1 \times 10^{-20*}$	[96]
$\text{CN} + \text{Ar}$	-130	$1 \times 10^{-20*}$	100	$1 \times 10^{-28*}$	[96]
Anions					
$\text{C}_2^- + \text{He}$	-30	1.4×10^{-6}	100	5.4×10^{-17}	This work
$\text{C}_2^- + \text{Ne}$	-110	3.8×10^{-6}	100	4.9×10^{-17}	This work
$\text{C}_2^- + \text{Ar}$	-490	7.2×10^{-2}	100	3.7×10^{-14}	This work

VI. CONCLUSIONS

The cross sections and corresponding thermal rates for rovibrationally inelastic collisions of C_2^- with He, Ne, and Ar have been calculated using a set of *ab initio* PESs. The rotationally inelastic vibrationally elastic cross sections were found to be insensitive to vibrational state, justifying the treatment of the C_2^- molecule as a rigid rotor [49,50]. The cross sections and rates for vibrational quenching from the $\nu = 1$ and 2 states for He and Ne were found to be orders of magnitude lower than those obtained for purely rotationally inelastic collisions. The values of the vibrational quenching rates are found for this anion to be similar in size to those known for other small neutral molecules in collision with helium atoms. For the Ar partner, the vibrationally inelastic rates we have obtained here were around three or four orders of magnitude larger.

These computed rate coefficients for vibrational quenching can be used to model the behavior of C_2^- in ion traps with He, Ne, or Ar as buffer gas. It turns out, in fact, that they have significant implications for laser cooling of C_2^- : the

inefficiency of vibrational quenching found for He and Ne in our calculations shows how important the knowledge of vibrational repumping rate coefficients is for modeling the cyclic scattering of many photons off C_2^- . To quench the states which are being populated within that cycle by using buffer gas collisions, as discussed in this study, will require higher pressures in order to efficiently increase the collision frequency in the trap. Our results suggest, therefore, that argon would be a more suitable buffer gas to efficiently quench the vibrational motion of C_2^- as lower pressures will be required for it as a buffer gas in comparison to using either helium or neon.

ACKNOWLEDGMENTS

We acknowledge the financial support of the Austrian FWF agency through research Grant No. P29558-N36. One of us (L.G.-S.) further thanks MINECO (Spain) for Grants No. CTQ2015-65033-P and No. PGC2018-09644-B-100. We are grateful for helpful discussions with G. Worth.

-
- [1] M. Tarbutt, *Contemp. Phys.* **59**, 356 (2018).
 - [2] J. Barry, D. McCarron, E. Norrgard, M. Steinecker, and D. DeMille, *Nature (London)* **512**, 286 (2014).
 - [3] F. Wolf, Y. Wan, J. C. Heip, F. Gerbert, C. Shi, and P. O. Schmidt, *Nature (London)* **530**, 457 (2016).
 - [4] H. Loh, K. C. Cossel, M. C. Grau, K. K. Ni, E. R. Meyer, J. L. Bohn, J. Ye, and E. A. Cornell, *Science* **342**, 1220 (2013).
 - [5] A. D. Dörfler, P. Eberle, D. Koner, M. Tomza, M. Meuwly, and S. Willitsch, *Nat. Commun.* **10**, 5429 (2019).
 - [6] P. Yzombard, M. Hamamda, S. Gerber, M. Doser, and D. Comparat, *Phys. Rev. Lett.* **114**, 213001 (2015).
 - [7] Y. Shan-Shan, Y. Xiao-Hua, L. Ben-Xi, K. Kakule, W. Sheng-Hai, G. Ying-Chun, L. Yu-Yan, and C. Yang-Qin, *Chin. Phys.* **12**, 745 (2003).
 - [8] W. Shi, C. Li, H. Meng, J. Wei, L. Deng, and C. Yang, *Comput. Theor. Chem.* **1079**, 57 (2016).
 - [9] J. Fesel, S. Gerber, M. Doser, and D. Comparat, *Phys. Rev. A* **96**, 031401(R) (2017).

- [10] S. Gerber, J. Fesel, M. Doser, and D. Comparat, *New J. Phys.* **20**, 023024 (2018).
- [11] M. Ahmadi, B. X. R. Alves, C. J. Baker, W. Bertsche, E. Butler, A. Capra, C. Carruth, C. L. Cesar, M. Charlton, S. Cohen *et al.*, *Nature (London)* **541**, 506 (2017).
- [12] P. Perez and Y. Sacquin, *Classical Quantum Gravity* **29**, 184008 (2012).
- [13] G. Herzberg and A. Lagerqvist, *Can. J. Phys.* **46**, 2363 (1968).
- [14] E. D. Milligan and M. E. Jacox, *J. Chem. Phys.* **51**, 1952 (1969).
- [15] R. P. Frosch, *J. Chem. Phys.* **54**, 2660 (1971).
- [16] W. C. Lineberger and T. A. Patterson, *Chem. Phys. Lett.* **13**, 40 (1972).
- [17] P. L. Jones, R. D. Mead, B. E. Kohler, S. D. Rosner, and W. C. Lineberger, *J. Chem. Phys.* **73**, 4419 (1980).
- [18] S. Leutwyler, J. P. Maier, and L. Misev, *Chem. Phys. Lett.* **91**, 206 (1982).
- [19] R. D. Mead, U. Hefter, P. A. Schulz, and W. C. Lineberger, *J. Chem. Phys.* **82**, 1723 (1985).
- [20] B. D. Reh fuss, D.-J. Liu, B. M. Dinelli, M.-F. Jagod, W. C. Ho, M. W. Crofton, and T. Oka, *J. Chem. Phys.* **89**, 129 (1988).
- [21] K. M. Ervin and W. C. Lineberger, *J. Phys. Chem.* **95**, 1167 (1991).
- [22] P. Royen and M. Zackrisson, *J. Mol. Spectrosc.* **155**, 427 (1992).
- [23] E. d. Beer, Y. Zhao, I. Yourshaw, and D. M. Neumark, *Chem. Phys. Lett.* **244**, 400 (1995).
- [24] H. B. Pedersen, C. Brink, L. H. Andersen, N. Bjerre, P. Hvelplund, D. Kella, and H. Shen, *J. Chem. Phys.* **109**, 5849 (1998).
- [25] A. E. Bragg, R. Wester, A. V. Davis, A. Kammrath, and D. M. Neumark, *Chem. Phys. Lett.* **376**, 767 (2003).
- [26] M. Nakajima, *J. Mol. Spectrosc.* **331**, 106 (2017).
- [27] E. S. Endres, O. Lakhmanskaya, D. Hauser, S. E. Huber, T. Best, S. S. Kumar, M. Probst, and R. Wester, *J. Phys. Chem. A* **118**, 6705 (2014).
- [28] J. Barsuhn, *J. Phys. B: At., Mol. Opt. Phys.* **7**, 155 (1974).
- [29] M. Zeitz, S. D. Peyerimhoff, and R. J. Buenker, *Chem. Phys. Lett.* **64**, 243 (1979).
- [30] M. Dupuis and B. Liu, *J. Chem. Phys.* **73**, 337 (1980).
- [31] P. Rosmus and H.-J. Werner, *J. Chem. Phys.* **80**, 5085 (1984).
- [32] J. A. Nichols and J. Simons, *J. Chem. Phys.* **86**, 6972 (1987).
- [33] J. D. Watts and R. J. Bertlett, *J. Chem. Phys.* **96**, 6073 (1992).
- [34] T. Šedivcová and V. Špirko, *Mol. Phys.* **104**, 1999 (2006).
- [35] M. Kas, J. Loreau, J. Liévin, and N. Vaeck, *Phys. Rev. A* **99**, 042702 (2019).
- [36] S. Gulania, T.-C. Jagau, and A. I. Krylov, *Faraday Discuss.* **217**, 514 (2019).
- [37] D. L. Lambert, Y. Sheffer, and S. R. Federman, *Astrophys. J.* **438**, 740 (1995).
- [38] D. L. Lambert, Y. Sheffer, A. C. Danks, C. Arpigny, and P. Magain, *Astrophys. J.* **353**, 640 (1990).
- [39] S. P. Souza and B. L. Lutz, *Astrophys. J.* **216**, L49 (1977).
- [40] D. L. Lambert, B. Gustafsson, K. Eriksson, and K. H. Hinkle, *Astrophys. J. Suppl. Ser.* **62**, 373 (1986).
- [41] M. S. Vardya and K. S. Krishna Swamy, *Chem. Phys. Lett.* **73**, 616 (1980).
- [42] T. Faj and H. R. Johnson, *Publ. Astronom. Soc. Pac.* **84**, 284 (1972).
- [43] G. Wallerstein, *Astron. Astrophys.* **105**, 219 (1982).
- [44] S. Civiš, Y. Hosaki, E. Kagi, H. Izumiura, K. Yanagisawa, T. Šedivcová, and K. Kawaguchi, *Publ. Astron. Soc. Jpn.* **57**, 605 (2005).
- [45] R. Wester, *J. Phys. B: At., Mol. Opt. Phys.* **42**, 154001 (2009).
- [46] F. A. Gianturco, L. González-Sánchez, B. P. Mant, and R. Wester, *J. Chem. Phys.* **151**, 144304 (2019).
- [47] A. Hinterberger, S. Gerber, E. Oswald, C. Zimmer, J. Fesel, and M. Doser, *J. Phys. B: At., Mol. Opt. Phys.* **52**, 225003 (2019).
- [48] A. K. Hansen, O. O. Versolato, L. Kłosowski, S. B. Kristensen, A. Gingell, M. Schwarz, K. Windberer, K. Ullrich, J. R. Crespo López-Urrutia, and M. Drewsen, *Nature (London)* **508**, 76 (2014).
- [49] B. P. Mant, F. A. Gianturco, L. González-Sánchez, E. Yurtsever, and R. Wester, *J. Phys. B: At., Mol. Opt. Phys.* **53**, 025201 (2020).
- [50] B. P. Mant, F. A. Gianturco, R. Wester, E. Yurtsever, and L. González-Sánchez, *J. Int. Mass Spectrom.* **457**, 116426 (2020).
- [51] R. J. Le Roy, *J. Quant. Spectrosc. Radiat. Transfer* **186**, 158 (2017).
- [52] R. J. Le Roy, *J. Quant. Spectrosc. Radiat. Transfer* **186**, 167 (2017).
- [53] See Supplemental Material at <http://link.aps.org/supplemental/10.1103/PhysRevA.102.062810> for details of the C₂⁻ PEC fit and vibrational wave functions, Fortran programs for the 2D C₂⁻-He/Ne/Ar rigid rotor PES and Legendre expansion parameters, Fortran programs for the 3D C₂⁻-He/Ne/Ar interaction potential, and Legendre expansions of the matrix elements of these surfaces.
- [54] P. R. Bunker, *Chem. Phys. Lett.* **27**, 322 (1974).
- [55] F. O. Ellison, *J. Chem. Phys.* **36**, 478 (1962).
- [56] A. Ishikawa, H. Nakashima, and H. Nakatsuji, *Chem. Phys.* **401**, 62 (2012).
- [57] F. Dumouchel, A. Spielfiedel, M. Senent, and N. Feautrier, *Chem. Phys. Lett.* **533**, 6 (2012).
- [58] S. Brünken, C. A. Gottlieb, H. Gupta, M. C. McCarthy, and P. Thaddeus, *Astron. Astrophys.* **464**, L33 (2007).
- [59] H.-J. Werner, P. J. Knowles, G. Knizia, F. R. Manby, and M. Schütz, *WIREs Comput. Mol. Sci.* **2**, 242 (2012).
- [60] H.-J. Werner, P. J. Knowles, G. Knizia, F. R. Manby, M. Schütz *et al.*, MOLPRO, version 2019.2, a package of *ab initio* programs see, <https://www.molpro.net>.
- [61] H. J. Werner and P. J. Knowles, *J. Chem. Phys.* **82**, 5053 (1985).
- [62] P. J. Knowles and H. J. Werner, *Chem. Phys. Lett.* **115**, 259 (1985).
- [63] K. R. Shamasundar, G. Knizia, and H.-J. Werner, *J. Chem. Phys.* **135**, 054101 (2011).
- [64] R. A. Kendall, T. H. Dunning Jr., and R. J. Harrison, *J. Chem. Phys.* **96**, 6796 (1992).
- [65] P. J. Knowles, C. Hampel, and H.-J. Werner, *J. Chem. Phys.* **99**, 5219 (1993).
- [66] M. J. O. Deegan and P. J. Knowles, *Chem. Phys. Lett.* **227**, 321 (1994).
- [67] A. K. Wilson, T. van Mourik, and T. H. Dunning Jr., *J. Mo. Struct.: THEOCHEM.* **388**, 339 (1996).
- [68] D. E. Woon and T. H. Dunning Jr., *J. Chem. Phys.* **98**, 1358 (1993).

- [69] S. F. Boys and F. Bernardi, *Mol. Phys.* **19**, 553 (1970).
- [70] H.-J. Werner, B. Follmeg, and M. Alexander, *J. Chem. Phys.* **89**, 3139 (1988).
- [71] C. Balança and F. Dayou, *Mon. Not. R. Astron. Soc.* **469**, 1673 (2017).
- [72] C. Gaiser and B. Fellmuth, *Phys. Rev. Lett.* **120**, 123203 (2018).
- [73] D. López-Duránn, E. Bodo, and F. A. Gianturco, *Comput. Phys. Commun.* **179**, 821 (2008).
- [74] A. M. Arthurs and A. Dalgarno, *Proc. R. Soc. A* **256**, 540 (1960).
- [75] D. E. Manolopoulos, *J. Chem. Phys.* **85**, 6425 (1986).
- [76] R. Martinazzo, E. Bodo, and F. A. Gianturco, *Comput. Phys. Commun.* **151**, 187 (2003).
- [77] I. Iskandarov, F. A. Gianturco, M. Hernández Vera, R. Wester, H. da Silva Jr., and O. Dulieu, *Eur. Phys. J. D* **71**, 141 (2017).
- [78] R. V. Krems, *J. Chem. Phys.* **116**, 4517 (2002).
- [79] F. Lique, A. Spielfiedel, G. Dhont, and N. Feautrier, *Astron. Astrophys.* **458**, 331 (2006).
- [80] F. Lique and A. Spielfiedel, *Astron. Astrophys.* **462**, 1179 (2007).
- [81] R. Tobała, F. Lique, J. Kłos, and G. Chałasiński, *J. Phys. B: At., Mol. Opt. Phys.* **41**, 155702 (2008).
- [82] R. V. Krems and S. Nordholm, *J. Chem. Phys.* **115**, 257 (2001).
- [83] R. V. Krems, N. Marković, A. A. Buchachenko, and S. Nordholm, *J. Chem. Phys.* **114**, 1249 (2001).
- [84] F. Naja, D. B. Abdallah, N. Jaidan, and B. Lakhdar, *Chem. Phys. Lett.* **460**, 31 (2008).
- [85] F. George D.X. and S. Kumar, *Chem. Phys.* **373**, 211 (2010).
- [86] B. Anusuri and S. Kumar, *J. Chem. Sci.* **128**, 287 (2016).
- [87] V. C. Saheer and S. Kumar, *J. Chem. Phys.* **144**, 024307 (2016).
- [88] F. G. D. Xavier and S. Kumar, *Phys. Rev. A* **83**, 042709 (2011).
- [89] B. K. Kendrick, *J. Phys. Chem. A* **123**, 9919 (2019).
- [90] B. K. Kendrick, *J. Chem. Phys.* **148**, 044116 (2018).
- [91] B. K. Kendrick, J. Hazra, and N. Balakrishnan, *J. Chem. Phys.* **145**, 164303 (2016).
- [92] Y. V. Suleimanov and T. V. Tscherebul, *J. Phys. B: At., Mol. Opt. Phys.* **49**, 204002 (2016).
- [93] M. Morita, R. V. Krems, and T. V. Tscherebul, *Phys. Rev. Lett.* **123**, 013401 (2019).
- [94] S. Kato, V. M. Bierbaum, and S. R. Leone, *Int. J. Mass Spec. Ion Proc.* **149-150**, 469 (1995).
- [95] E. E. Ferguson, *J. Phys. Chem.* **90**, 731 (1986).
- [96] G. Saidani, Y. Kalugina, A. Gardez, L. Biennier, R. Georges, and F. Lique, *J. Chem. Phys.* **138**, 124308 (2013).
- [97] T. Stoecklin and A. Voronin, *J. Chem. Phys.* **134**, 204312 (2011).
- [98] D. Caruso, M. Tacconi, F. A. Gianturco, and E. Yurtsever, *J. Chem. Sci.* **124**, 93 (2012).
- [99] T. Stoecklin and A. Voronin, *Eur. Phys. J. D* **46**, 259 (2008).
- [100] T. Stoecklin, P. Halvick, M. A. Gannounim, M. Hochlaf, S. Kotochigova, and E. R. Hudson, *Nat. Commun.* **7**, 11234 (2016).
- [101] W. C. Campbell, G. C. Groenenboom, H.-I. Lu, E. Tsikata, and J. M. Doyle, *Phys. Rev. Lett.* **100**, 083003 (2008).
- [102] I. Kozyryev, L. Baum, K. Matsuda, P. Olson, B. Hemmerling, and J. M. Doyle, *New J. Phys.* **17**, 045003 (2015).
- [103] W. Rellergent, S. S. S. Schowalter, S. Kotochigova, K. Chen, and E. R. Hudson, *Nature (London)* **495**, 490 (2013).